Available online at www.sciencedirect.com
ScienceDirect
Energy Conversion and Management 48 (2007) 2864–2878
ENERGY CONVERSION & MANAGEMENT
www.elsevier.com/locate/enconman

Analysis of thermal cycles and working fluids for power generation in space

Jason Tarlecki [a], Noam Lior [a,*], Na Zhang [b]

[a] Department of Mechanical Engineering and Applied Mechanics, University of Pennsylvania, Philadelphia, PA 19104-6315, USA
[b] Institute of Engineering Thermophysics, Chinese Academy of Sciences, Beijing 100080, China

Available online 30 August 2007

Abstract

Production of power in space for terrestrial use is of great interest in view of the rapidly rising power demand and its environmental impacts. Space also offers a very low temperature, making it a perfect heat sink for power plants, thus offering much higher efficiencies. This paper focuses on the evaluation and analysis of thermal Brayton, Ericsson and Rankine power cycles operating at space conditions on several appropriate working fluids. Under the examined conditions, the thermal efficiency of Brayton cycles reaches 63%, Ericsson 74%, and Rankine 85%. These efficiencies are significantly higher than those for the computed or real terrestrial cycles: by up to 45% for the Brayton, and 17% for the Ericsson; remarkably 44% for the Rankine cycle even when compared with the best terrestrial combined cycles. From the considered working fluids, the diatomic gases (N_2 and H_2) produce somewhat better efficiencies than the monatomic ones in the Brayton and Rankine cycles. The Rankine cycles require radiator areas that are larger by up to two orders of magnitude than those required for the Brayton and Ericsson cycles. The results of the analysis of the sensitivity of the cycle performance parameters to major parameters such as turbine inlet temperature and pressure ratio are presented, equations or examining the effects of fluid properties on the radiator area and pressure drop were developed, and the effects of the working fluid properties on cycle efficiency and on the power production per unit radiator area were explored to allow decisions on the optimal choice of working fluids.

Keywords: Power cycles; Space power; Space; Brayton cycle; Ericsson cycle; Rankine cycle

1. Power from space

In view of the worrisome fact that the world population is expected to double and the demand for electricity to increase 16-fold in the next 50 years, it was recognized over the past few decades by various scientific and aerospace experts and institutions [1–4] that space offers numerous advantages as a site for power production. This approach has many advantages, as well as serious obstacles, described briefly below. In addition to the better known proposal to generate power in space by using photovoltaic converters [1], an important advantage of space is also an ideal, near-zero K, heat sink for thermal power generation, and can thus offer Carnot efficiencies close to 100% [4]. Exploiting this low temperature in space, working fluids can be used in the power plant (such as inert gas mixtures), even to condensation in the Rankine cycle.

Some of the most probable heat sources are solar and nuclear. Using the sun as the primary energy source of the power plant only further boosts the advantages of power from space solar power, which requires a collection area about 8-fold smaller than that needed on earth [1,5–7]. Nuclear energy, already used for satellite and space probe powering in space over the last 30 years, is also an option for space. The nuclear sources include radioisotope systems and fission reactors, with the latter having the highest specific energy (kJ/kg) content of all fuels [4].

Some of the most likely methods for transmitting the generated energy to earth are microwave or laser beaming, and transportation of energy-rich materials. Being able to beam the energy to the location needing it, the use of space

* Corresponding author. Tel.: +1 215 898 4803; fax: +1 215 573 6334.
E-mail address: lior@seas.upenn.edu (N. Lior).

0196-8904/$ - see front matter © 2007 Elsevier Ltd. All rights reserved.
doi:10.1016/j.enconman.2007.06.039

Nomenclature

A	area [m^2]
a	exergy [kJ/kg]
c	speed of sound [m/s]
c_p	constant pressure specific heat [kJ/kg K]
c_v	constant volume specific heat [kJ/kg K]
D	characteristic diameter [m]
G	mass flow rate [kg/s]
HE	regenerator
HS	heat source generator
h	enthalpy [kJ/kg]
h_c	convective heat transfer coefficient [W/m^2 K]
h_r	radiative heat transfer coefficient [W/m^2 K]
k	thermal conductivity constant [W/m K]
L	characteristic length [m]
LEO	low earth orbit
MC	multistage compressor
MT	multistage turbine
Nu	Nusselt number
N	generator
p	pressure [bar]
Pr	Prandtl number
Q	heat duty [kW]
R	radiator
Re	Reynolds number
R_t	total thermal resistance [K/W]
s	specific entropy [kJ/kg K]
t	radiator wall thickness [m]
T	temperature [K]
TIT	turbine inlet temperature [K]
U	overall heat transfer coefficient [W/m^2 K]
v	velocity [m/s]
W	power output [kW]
w	specific power output [kJ/kg]

Greek

δ	radiator flow gap [m]
ΔT_{lm}	log mean temperature difference [K]
ϵ	emittance
ε	exergy efficiency
η_I	thermal efficiency
π	pressure ratio
ρ	density [kg/m^3]
σ_{sb}	Stefan–Boltzmann constant [$5.67(10^{-8})$ W/m^2 K^4]
Ψ	power produced per unit radiator area [kW/m^2]

Subscripts

in	inlet
out	outlet
H	high
L	low
rad	radiator
s	space
t	total
1…10	states on the cycle flow sheet

power improves power distribution as there is less need for pipelines, tankers, and electric power lines that require land-use and/or incur resistance losses. Wireless power transmission, an integral part of these space power systems, is continually improving [5,6]. Ground tests have shown that wireless energy transmission can be achieved at high efficiencies (75–82%) [6,8,9].

In addition to the advantages of year round availability of solar energy, practically around the clock, and at a higher intensity than on earth, the advantages of using space for power generation include sparing the precious terrestrial surface that would have been used for situation of power plants, which is especially large where renewable energy is planned to be used, and avoidance of the direct terrestrial pollution consequences from the terrestrial power plants. Space power plants would not be exposed to high gravity, wind, earthquakes, rust, or corrosion, dust, hail or vandalism. Consequently, power systems in space can be constructed of much lighter (and therefore cheaper) materials. In terms of safety, power plant dangers such as fire, explosion, or the spread of harmful materials will be much less of a threat (if any) to Earth and its inhabitants. Obviously there also exist some important challenges is establishing such plants, including the high cost (presently estimated to be two orders of magnitude higher than that of conventional terrestrial power) and energy needed to transport the power plant components into space and to construct and maintain the plant there, experience with large scale power transmission from the space station to earth, environmental issues, primarily related to power transmission and to launch vehicle emissions, but also resulting from manufacturing of the power plant, space plant security, absence and complexities of international agreements on space use and power distribution, and damage from meteorites and under space objects [4,5].

Globally, power generation in space for terrestrial use can help meet the increasing power demands due to the increasing population and its aspiration for a better standard of living, especially in developing nations whose power demands are increasing very rapidly and are expected to become the greatest in the coming decades [6,10–12]. It will be more efficient to beam this power to developing countries, instead of building new power lines, similar to how cellular phones have surpassed conventional telephones in these regions. Obviously, the utility of space power for developing nations, just as for the developed ones, is reduction of cost to acceptable levels, and the establishment of reliable and equitable international agree-

ments. Although it is quite obvious that a project of this size will require large amounts of energy, especially for the materials of these space structures and the fuel used to power the launchings, studies conducted so far argue that long-term payoff makes it worth the investment. For example, the energetic amortization time, or the required operating time for a solar power satellite to pay back the energy needed for its production, fabrication, and operation, was estimated to be of the order of two years [13]. Furthermore, "maintaining a level playing field" is crucial, meaning that all environmental consequences of conventional power production should be weighed when comparing to the literal high cost of space power.

2. The objective of this study: Analysis of thermal power cycles for use in space

The possible use of thermal space power cycles requires developments in many areas, and this paper deals with one aspect of space power generation: the analysis of performance of recuperative Brayton, Ericsson, and Rankine thermal power cycles that operate under space conditions. The heat source could be any, most likely solar or nuclear, and space is the heat sink.

The primary obstacle to commercial use of space power is the high cost of the produced power, which, in turn, is strongly affected by the system weight because sending the systems into space with currently available launch systems is a dominant fraction of the total cost [14,15]. For a desired net power output, increasing the thermal system energy conversion efficiency reduces both the cost of the heat input system (solar concentrator and receiver, or nuclear reactor) and the amount of heat that must be rejected (and thus the size and weight of the radiator). At the same time, reduction of the working fluid temperature in the radiator increases the thermal efficiency but decreases the heat rejection temperature difference and consequently increases the needed radiator size/weight, requiring optimization of that temperature.

The temperature and pressure of space are needed for setting the heat sink temperature, designing of the heat rejection radiator, and establishing the dead state in the exergy analysis. Currently, astronomers agree that the cold temperature of space is about 3 K. In this analysis, it is estimated to be 2.7 K due to background microwave radiation [16,17], but varying the temperature by a few degrees does not affect the results significantly. This temperature is assumed here to be the lowest that space can offer and is thus useful for estimating the maximal thermodynamic potential of space, and is used here as the dead state temperature for the exergy analysis. It is noteworthy though that the effective temperature depends on the radiative exposure to nearby objects, and the literature shows use of space temperatures from 0 K [18] to 223 K [19], with a value of ~190 K used often.

The pressure environment is complex and can fluctuate substantially. At a height of 320 km (in Low Earth Orbit, LEO) from Earth's surface, an orbiting object can be in a pressure field varying between 10^{-8} bar in the front to 10^{-10} bar in the rear due to collisions with the ambient atmosphere. Assuming an orbital velocity of about 8 km/s, the dead state pressure (p_0) becomes 10^{-8} bar [19]. The moon may also be an option for space power, having dead state pressure of 3×10^{-15} bar and a mean diurnal temperature range from 100 to 400 K [20].

The top cycle temperatures were selected to be those employed in conventional power plants, and somewhat beyond, to address expected increases as technology keeps developing. The very low bottom cycle temperature (below 100 K in Rankine cycles) and the correspondingly high temperature ratio make the performance of these cycles rather interesting.

Three primary performance criteria were used for evaluating and comparing the different cycles and working fluids: the energy efficiency η_I, the exergy efficiency ε (very useful for helping find ways to improve cycle performance), and the ratio of the power output to required radiator area, Ψ [kW/m^2], which are defined, respectively, as

$$\eta_I = \frac{w_{\text{net}}}{Q_{\text{in}}} \tag{1}$$

$$\varepsilon = \frac{w_{\text{net}}}{(a_{\text{out}} - a_{\text{in}})_{\text{heat-addition}}} \tag{2}$$

$$\Psi = \frac{G w_{\text{net}}}{A_{\text{rad}}} \tag{3}$$

3. Radiator analysis

Beside the system efficiencies, the radiator area becomes an important constraint especially since costs of bringing matter into space are extremely high. The conceived radiator for all three cycles is of a flat-plate design. It is assumed that the radiators will be constructed of aluminum, to cohere with similar space power structures [21,22]. The necessary radiator area needed to reject the heat rate Q_{out} is calculated from

$$A_{\text{rad}} = \frac{Q_{\text{out}}}{U \Delta T_{\text{lm}}} \tag{4}$$

The overall heat transfer coefficient (U) is calculated from

$$U = \frac{1}{R_t A} = \frac{1}{t/k + 1/h_c + 1/h_r} \tag{5}$$

where k is the thermal conductivity of the plate, t its thickness, h_c the convective heat transfer coefficient, and h_r the radiative heat transfer coefficient calculated here by

$$h_r \equiv \epsilon \sigma_{sb} (\Delta T_{\text{lm}} + T_s)(\Delta T_{\text{lm}}^2 + T_s^2) \tag{6}$$

The required size of the radiators is calculated from Eq. (4), rewritten as

$$A_{\text{rad}} = \frac{G c_{p,6-1}(T_6 - T_1)}{U \Delta T_{\text{lm}}} \tag{7}$$

Using Eqs. (3), (7), (1), Ψ can be expressed as

$$\Psi = \frac{Gw_{\text{net}}}{A_{\text{rad}}} = U\Delta T_{\text{lm}} \frac{w_{\text{net}}}{q_{\text{out}}} = U\Delta T_{\text{lm}} \frac{1}{\frac{1}{\eta_I} - 1} \tag{8}$$

indicating, as expected, that Ψ will decrease if U and ΔT_{lm}, are increased, and if the energy efficiency of the cycle, η_I, is increased. Eq. (8) is strictly valid for Brayton and Rankine cycles only, as the Ericsson cycle has multiple radiators, with varying ΔT_{lm} and U throughout multiple stages of heat rejection.

4. Cycle configurations

The configurations for the Brayton, Ericsson and Rankine cycles analyzed in this paper are shown in Figs. 1–3, respectively. Since this is just an initial study, simple configurations were chosen. The *Brayton* cycle is self-explanatory. It is common practice to use intercoolers and reheat stages in gas cycle power plants, which is the basic principle of the *Ericsson* cycle that was studied here. The studies were however, for a finite number of compression and expansion stages, as chosen and described in the Section "Power Generation" below. In the *Ericsson* cycle, the gas at state (1) enters a multistage compressor (MC) where it is compressed and intercooled several times to mimic constant temperature compression. At state (2), the gas enters the HE, is heated to state (3), then is further heated in a heat source generator (HS). The high temperature and pressure gas (4) enters a multistage turbine (MT) and is expanded and reheated multiple times until the entire process approaches constant temperature expansion and reaches state (5). Here the gas enters the regenerator (HE) where the heat remaining from the constant temperature expansion is transferred to the cooler gas at state (2). At state (6), the gas is further cooled in the radiator (R) until reaching its original state (1).

The *Rankine* cycle is perhaps the most interesting of the three explored, because the low temperature of space is used to liquefy the inert gases used, resulting in the lowest required back-work ratio. The vapor exiting the regenerator at state (6) is condensed in the radiator (R), where the heat is rejected to space, bringing the working fluid back to its original state (1).

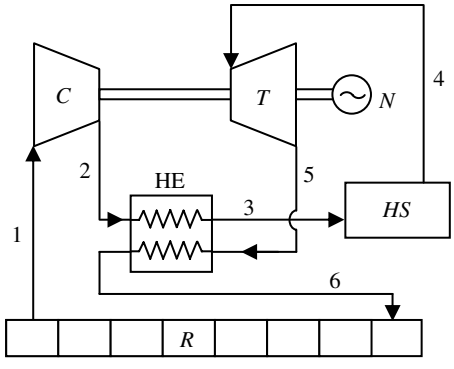

C— Compressor *T*— Turbine *HE*— Heat Exchanger
N— Generator *HS*— Heat Source *R*— Radiator

Fig. 1. Brayton cycle flow sheet.

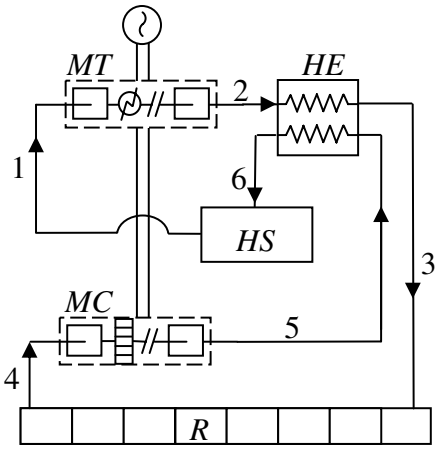

MC— Multistage Compressor w/ Intercooling
MT— Multistage Turbine w/ Reheating *N*— Generator
HE— Heat Exchanger *HS*— Heat Source *R*— Radiator

Fig. 2. Ericsson cycle flow sheet.

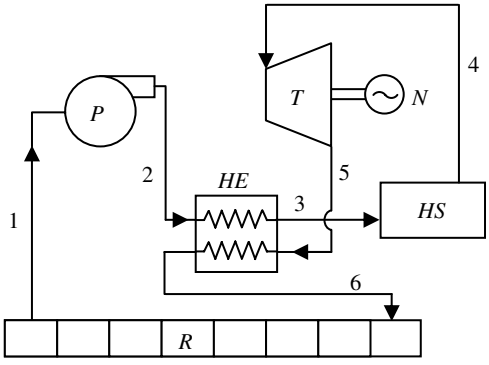

P— Pump *T*— Turbine *HE*— heat exchanger
N— Generator *HS*— Heat Source *R*— Radiator

Fig. 3. Rankine cycle flow sheet.

5. Selection of working fluids

Based on past work on space thermal power cycles [21–26], the working fluids investigated for the Brayton and Ericsson cycles are argon (Ar), nitrogen (N_2), argon–xenon (Ar–Xe, 50% Ar by weight), helium (He), helium–xenon (He–Xe, 50% He by weight), and hydrogen (H_2). Only the first two fluids were considered for the Rankine cycle. The major properties of the fluids, for the considered range of the lower (heat rejection) and higher (heat addition) parts of the cycles are given in Tables 1a and 1b. The exposition of the properties is important for clarifying the relative suitability of working fluids.

Brayton and Ericsson cycle performance improves significantly as the compressor inlet temperature decreases, and to take the advantage of the very low heat sink

Table 1a
Major properties of the considered working fluids for the conditions of the analyzed Brayton and Ericsson cycles

The working fluid			Ar	He	Xe	Ar–Xe	He–Xe	N_2	H_2
Condensation		T, K	84.5	–	–	–	–	64.2	–
		P, bar	0.75	–	–	–	–	0.15	–
Triple point		T, K	83.80	2.17	161.3	–	–	63.15	13.95
		P, bar	0.69	0.05	0.82	–	–	0.13	0.07
Critical point		T, K	150.7	5.20	289.7	–	–	126.2	33.19
		P, bar	48.6	2.27	58.4	–	–	34.0	13.2
Speed of sound*		c, m/s	721	2261	396	578	1626	760	2867
Atomic mass			39.95	4.00	131.29	61.26	7.76	28.01	2.02
Property	P, bar	T, K							
c_p, kJ/kg K	1	200	0.524	5.194	0.162	0.342	2.676	1.044	13.91
		300	0.522	5.194	0.160	0.341	2.676	1.042	14.28
		500	0.521	5.193	0.159	0.340	2.676	1.057	14.54
	8	700	0.522	5.194	0.160	0.341	2.676	1.100	14.58
		1500	0.521	5.193	0.159	0.340	2.676	1.244	16.00
$(1 - c_v/c_p)$	1	200	0.403	0.401	0.412	0.405	0.401	0.289	0.297
		300	0.402	0.400	0.405	0.402	0.401	0.287	0.289
		500	0.401	0.400	0.402	0.401	0.400	0.282	0.284
	8	700	0.401	0.401	0.405	0.402	0.401	0.271	0.283
		1500	0.400	0.400	0.401	0.400	0.400	0.239	0.258
$k \times 10^6$, kW/m K	1	200	13	118	4	10	106	18	130
		300	18	150	6	14	140	26	180
		500	27	219	9	21	201	39	266
	8	700	34	280	12	27	250	51	340
		1500	57	480	22	47	440	93	610
ρ, kg/m^3	1	200	2.4109	0.2407	8.0308	3.7053	0.4672	1.6893	0.1212
		300	1.6030	0.1604	5.2950	2.4601	0.3114	1.1236	0.0808
		500	0.9609	0.0963	3.1622	1.4737	0.1868	0.6737	0.0485
	8	700	5.4821	0.5498	18.087	8.4105	1.0671	3.8401	0.2766
		1500	2.5593	0.2566	8.4098	3.9241	0.4981	1.7942	0.1292
$v \times 10^7$, m^2/s	1	200	67	630	19	44	355	77	559
		300	140	1200	44	96	710	160	1100
		500	353	2951	117	242	1719	384	2619
	8	700	79	650	27	55	380	85	580
		1500	290	2400	100	200	1400	300	2100

The last 5 properties are given for the lower temperatures (heat rejection range, 200–500 K) and pressure $p_L = 1$ bar in a cycle, and for the higher ones (heat addition range, 700–1500 K, $p_H = 8$ bar).

* Property c evaluated at $p = 8$ bar and $T = 1500$ K.

temperature that space offers, the working fluids in gas cycles should thus have low condensation temperatures at the cycle low pressure.

In the Rankine cycle, the working fluid should have a low triple point temperature and pressure, to take advantage of the low heat sink temperature and enlarge the possible (T–s) working area of the fluid.

The conventional sub-critical Rankine cycles are not suitable for this application because their thermodynamic states are basically enclosed within the saturation curve, with the cycle high and low pressures between the critical pressure and the triple point pressure, respectively. It can be seen from Table 1a that the critical pressures of the working fluids considered in this paper are relatively low, so in this paper only supercritical Rankine cycles are considered, with the cycle high pressure set above the critical value.

To get a preliminary understanding of the efficiencies dependence on the type of working fluid, we can use a rough representation of the cycle performance as the equivalent Carnot efficiency

$$\eta_I = 1 - \frac{\widehat{T}_L}{\widehat{T}_H} \tag{9}$$

where $\widehat{T}_H$ and $\widehat{T}_L$ are the cycle average heat intake (path 3-4 in the Brayton and Rankine cycles, 3-4 and 4-5 [turbine reheat] Ericsson, Figs. 1–3) and rejection temperatures (6-1 in the Brayton and Rankine cycles, 6-1 and 1-2 [compressor intercooling] Ericsson), respectively. For all fluids, regeneration raises T_3, and thus also raises $\widehat{T}_H$, it lowers T_6 and thus lowers $\widehat{T}_L$, consequently increasing the efficiencies. Since turbine inlet temperature (TIT) is kept the same for all the fluids, the main effect on the efficiency would be that of $\widehat{T}_L$, which, besides by better regeneration, can be lowered by using a fluid with a: (1) lower condensation temperature, and (2) smaller temperature drop for the same expansion pressure ratio in the regeneration cycle. The latter can be explained by the isentropic relation for an

Table 1b
Major properties of the considered working fluids for the conditions of the analyzed Rankine cycle

Property	P, bar	T, K	Ar	N_2
c_p, kJ/kg K	0.15	64	–	1.860
		84	–	1.044
	0.75	84	1.042	1.063
		105	0.530	1.054
	150	200	1.342	1.743
		1500	0.524	1.247
$(1 - c_v/c_p)$	0.15	64	–	0.000
		84	–	0.289
	0.75	84	0.000	0.301
		105	0.410	0.295
	150	200	0.722	0.521
		1500	0.400	0.237
$k \times 10^6$, kW/m K	0.15	64	–	158
		84	–	8
	0.75	84	126	8
		105	7	10
	150	200	33	38
		1500	58	94
ρ, kg/m^3	0.15	64	–	866.6
		84	–	0.6046
	0.75	84	1416.4	3.0840
		105	3.4836	2.4403
	150	200	559.1	303.8
		1500	46.9	32.7
$v \times 10^7$, m^2/s	0.15	64	–	3
		84	–	97
	0.75	84	2	19
		105	25	30
	150	200	1	1
		1500	16	17

The last five properties are given for the lower temperatures (heat rejection range for Ar, 84–105 K, $p_L = 0.75$ bar; heat rejection range for N_2, 64–84 K, $p_L = 0.15$ bar), and heat addition range for both fluids, 200–1500 K, $p_H = 150$ bar.

expansion (or compression) process between inlet and outlet pressures p_{in} and p_{out}, respectively, of

$$T_{out} = T_{in}\left(\frac{p_{out}}{p_{in}}\right)^{1-\frac{c_v}{c_p}} \tag{10}$$

Although this equation is strictly valid only for constant specific heats, and an isentropic process, it gives good guidance about the dependence of the temperature change on the pressure ratio. For a constant pressure ratio (p_{out}/p_{in}), fluids which have a smaller value of the property $(1 - c_v/c_p)$ will thus exhibit a smaller temperature change ($T_{out} - T_{in}$) with same T_{in}. In the case of the Brayton cycles studied here, in which the work-producing and –consuming process are close to isentropic, fluids with a smaller value of $(1 - c_v/c_p)$ will during the expansion process in the turbine(s) (work-generation) for the same pressure ratio thus cool down to a higher temperature (e.g., T_5) when T_4 is held constant, and would thereby increase the cycle efficiency. In the compression process (wok-consuming), fluids with a smaller value of $(1 - c_v/c_p)$ will for the same pressure ratio compress to a lower temperature (e.g. T_2), and can thereby cool (by means of the regenerator HE) the turbine exhaust to a lower temperature (T_6), and therefore to lower T_L in the radiator (R), again tending to raise the efficiency.

$(1 - c_v/c_p)$ is plotted in Fig. 4 against T, showing that it is significantly higher for the monatomic than the diatomic gases considered here. Consequently, the Brayton cycle efficiencies when using N_2 or H_2 are expected to be higher than when using Ar or He.

In addition to the above-discussed specific heat *ratios* of the working fluids, the actual values of the specific heats are of importance in regard to cycle efficiencies and to heat transfer in the heat exchangers. Examining Table 1a, one can see that N_2 has a c_p that is more than 2-fold higher than that of Ar, but about 14-fold lower than that of H_2 and 4 to 5 fold lower than that of He.

Examination of the effects of fluid properties on the performance of the Ericsson cycle is somewhat more complex than that for the Brayton cycle, and can be done by examining the Ericsson cycle more explicit energy efficiency equation, where using the relationship $dh = c_p dT$, Eq. (1) becomes

$$\eta_I = \frac{w_{net}}{q_{in}} = \frac{nc_{p,H}\Delta T_H - nc_{p,L}\Delta T_L}{c_{p,H}\Delta T_{HS} + (n-1)c_{p,H}\Delta T_H} = \frac{1 - \frac{c_{p,L}\Delta T_L}{c_{p,H}\Delta T_H}}{\frac{\Delta T_{HS}}{n\Delta T_H} + \frac{n-1}{n}} \tag{11}$$

where n is the number of stages in either the turbine or the compressor, ΔT_H is the expansion (and reheat input) temperature difference between stages in the turbine, ΔT_L is the compression temperature difference of each stage in the compressor, and ΔT_{HS} is the temperature change in HS due to the heat input there (Fig. 2). Closely examining Eq. (11) to see its variance with different working fluids, and noting that n in our model remains constant for all working fluids, we first examine the numerator. Although the ratios $c_{p,L}/c_{p,H}$ and $\Delta T_L/\Delta T_H$ are different for monatomic and diatomic gases, the product of these ratios is

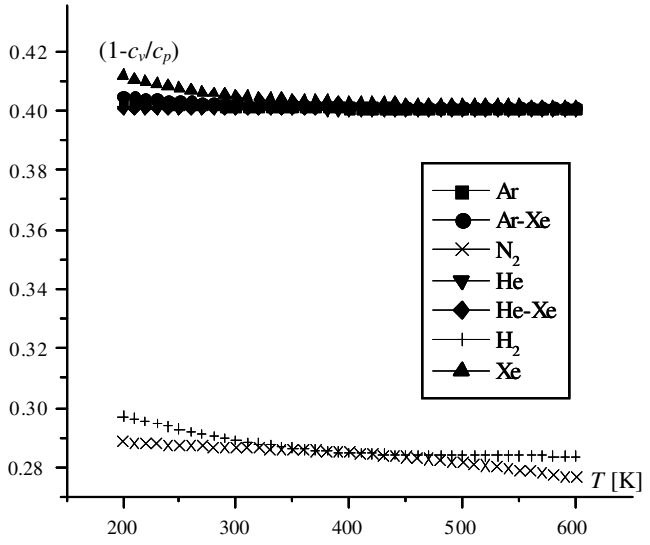

Fig. 4. The dependence of $(1 - c_v/c_p)$ on T for the considered working fluids, $p = 1$ bar.

near constant except when He is presented in the working fluid.

This has an important effect on the Ericsson cycle, in which the multistage expansion and compression take place over only small pressure differences, and the respective temperature drops and rises, respectively, become small (Eq. (10)), and thus may also become of smaller relative importance in their potential to lower $\widehat{T}_L/\widehat{T}_H$, than effect on efficiency of the heat input and rejection enthalpy differences $\Delta h = c_p \Delta T$ of the cycle.

The efficiency (η_C, Carnot) of lowering the bottom temperature $\widehat{T}_L$, as using space as the heat sink allows, in comparison with raising the top temperature $\widehat{T}_H$ can also be seen by examining the relationship $\frac{(d\eta_C/d\widehat{T}_L)}{(d\eta_C/d\widehat{T}_H)} = -\frac{\widehat{T}_H}{\widehat{T}_L}$ obtained from the Carnot efficiency Eq. (9). It is clear that the efficiency increase due to lowering $\widehat{T}_L$ is always larger than its increase due to similar raising of $\widehat{T}_H$ and the ratio is especially large when $\widehat{T}_L \to 0$.

The fluid properties also have an important role in the size of the equipment, especially the heat exchangers, and on the flow pressure drops through all of the fluid conduits. The primary properties affecting these components are the atomic mass, thermal conductivity, specific heat, density, and viscosity. Higher atomic weight working fluids allow the design of turbines of better performance, and xenon at an atomic mass of 131 is by far the heaviest (see Table 1), and this is why it is often mixed with other fluids for power generation applications. At the same time, it has, however, the lowest specific heat and a high value of $(1 - c_v/c_p)$. Also, the efficiency of turbines increases as the Mach number decreases, thus favoring fluids in which the speed of sound, c, is higher. As seen in Table 1a, H_2 and He have by far the highest values of c, followed closely by the He–Xe mixture.

The convective heat transfer coefficient between the fluid and its heat sinks and sources is a strong function of its thermal conductivity, and of the flow Reynolds number, which for the same velocity and characteristic diameter increases as the kinematic viscosity decreases. Higher thermal conductivities and lower kinematic viscosities thus result in: (1) smaller heat transfer area requirement, or/and (2) a closer approach to the heat sink and source temperatures thus resulting in a higher power generation efficiency (cf. Eq. (9)). In that respect, H_2 has the highest thermal conductivity (closely followed by He), being about 7 times higher than N_2, 10-fold higher than Ar and 30-fold higher than Xe. At the same time, Xe has the lowest kinematic viscosity, about 20-fold lower than those of H_2 and He.

An understanding of the role of properties on the pressure drop (Δp) can be explained from an examination of a generic equation used to calculate it for flow of a fluid of density ρ at velocity v through a conduit of characteristic diameter D and length L, such as

$$\Delta p = f \frac{L}{D} \frac{1}{2} \rho v^2 \tag{12}$$

where f is the friction factor, that can be approximated by $f = f(Re^{-b})$ and where b is coefficient depending on relative conduit roughness, $0 < b < 1$. For a given conduit geometry, v depends on the flow rate needed for a given enthalpy drop through the turbine, Δh (such as $h_4 - h_5$ in the cycles in Figs. 1 and 3), defined by the associated temperature drop ΔT, to produce a work output $\dot{W}_{out}$,

$$\dot{W}_{out} = \dot{m} \Delta h = \rho v A c_p \Delta T \tag{13}$$

where A is the conduit flow cross sectional area. Using this equation we get

$$v = \frac{\dot{W}_{out}}{A \Delta T \rho c_p} \tag{14}$$

Substituting this equation into (12) and using the above relationship for f gives

$$\Delta p \propto \frac{1}{2} \frac{L}{D} \left(\frac{\dot{W}_{out}}{A \Delta T} \right)^2 \frac{f \left(\frac{vD\rho}{\mu} \right)^{-b}}{\rho c_p^2} = K f (\rho^{-1} c_p^{b-2} \mu^b)$$
$$= K f (\rho^{b-1} c_p^{b-2} \nu^b) \tag{15}$$

where K is a constant which is fixed by the flow geometry and the given $\dot{W}_{out}$ and ΔT,

$$K \equiv \frac{1}{2} \frac{L}{D^{1+a}} \left(\frac{\dot{W}_{out}}{A \Delta T} \right)^{2-b} \tag{16}$$

Eq. (15) gives the quantitative dependence of the pressure drop on the fluid density, specific heat, and viscosity, and shows that it is lower for fluids with high density and specific heat and low viscosity. For example, if we take a typical value of $b = 0.2$, H_2 would give the lowest value of Δp, followed by He, and Xe the highest. Use of fluids of high density is favored also because it reduces the required flow cross section A, and system volume, since velocities are limited.

6. Performance of cycles

6.1. Cycle definitions and analysis method

To compute these and all the other system parameters, simulations of the systems were carried out using the Aspen Plus commercial software package [27] in which the component models are based on the energy balance and mass balance, with the relative convergence error tolerance of 10^{-5}. Both the internal and external irreversibilities were included in this model. All heat transfer through finite temperature differences and expansions of liquids and gases to lower pressures have been accounted for. The pressure drops in the pipes were, however, ignored to keep this analysis relatively simple and as close to ideal as possible. From power plant practice, they would be within roughly 3% pressure drop only anyway.

The same cycle configurations, using the same fluids, but under conventional terrestrial conditions were computed in the same way for comparison. For comparison to the ideal,

Table 2
All cycle parameters and results

			Brayton space	Brayton terrestrial	Ericsson space	Ericsson terrestrial	Rankine space	
							Ar	N_2
Cycle parameter		p_L [bar]	1	1	1	1	0.75	0.15
		T_L [K]	200	313.2	200	328.2*	84	64
Compression stage		π	8	8	8	8	200	1000
Carnot efficiency			0.8667	0.7912	0.8667	0.7912	0.9440	0.9573
Results	η_I	Ar	0.5826	0.4013	0.7364	0.6422	0.7788	
		Ar–Xe	0.5829	0.4014	0.7374	0.6427	–	
		N_2	0.6339	0.4949	0.6970	0.5946	0.8461	
		He	0.5818	0.4012	0.6684	0.6412	–	
		He–Xe	0.5819	0.4012	0.6709	0.6413	–	
		H_2	0.6322	0.4896	0.7035	0.6094	–	
	ε	Ar	0.5841	0.5423	0.7379	0.7947	0.7828	
		Ar–Xe	0.5844	0.5425	0.7389	0.7954	–	
		N_2	0.6354	0.6527	0.6983	0.7363	0.8496	
		He	0.5833	0.5422	0.6697	0.7935	–	
		He–Xe	0.5833	0.5422	0.6722	0.7936	–	
		H_2	0.6337	0.6489	0.7049	0.7545	–	
	Ψ [kW/m^2]	Ar	0.9958	–	0.4393	–	0.01435	
		Ar–Xe	0.9947	–	0.4376	–	–	
		N_2	0.8683	–	0.3921	–	0.00816	
		He	1.0014	–	0.3426	–	–	
		He–Xe	1.0013	–	0.3455	–	–	
		H_2	0.8499	–	0.3979	–	–	

$G = 350$ kg/hr, $\eta_S = 90\%$ (turbine), $\eta_S = 85\%$ (compressor, pump), $TIT = 1500$ K.
* Average temperature during compression with intercooling.

the Carnot efficiency was also computed. All the conditions and results are shown in Table 2. The computed values of T, h, and s at all the cycle states for all working fluids are shown in Tables 3–5 for the Brayton, Ericsson, and Rankine cycles, respectively.

To examine the limits of performance, high temperature and pressure ratios were used in the analysis, somewhat higher than used in conventional systems. Since this is a preliminary study, turbine blade cooling is not considered. The literature shows that blade cooling reduces a simple cycle efficiency by 2–3% points, and a recuperative cycle by up to 5% points. In conventional Rankine cycles the inlet steam pressure is 35–135 bar and the condensation pressure is about 0.05–0.07 bar, and thus the average pressure ratio is 1500 or even higher, and our study was for a pressure ratio of up to 1000.

Regeneration temperatures are determined by the compressor and turbine exit temperatures for the Brayton and Ericsson cycles, and by the turbine exit temperature and pinch point for the Rankine cycle. The heat exchanger HE effectiveness is chosen as 0.9, used in the Brayton and Ericsson cycles. However, in the Rankine cycle, an effectiveness of 0.9 cannot be achieved due to existence of liquid on the cold side of HE (process T_2 to T_3), causing the two stream temperatures to arrive at a pinch point before reaching this value of the effectiveness. Thus, in the Rankine cycle, a least temperature difference of 15 K is chosen to insure that most of the heat is exchanged without necessitating large HE areas.

6.2. Power generation

Fig. 5 shows the dependence of the energy efficiency and of Ψ, and Fig. 6 of the exergy efficiency, on the pressure ratio (π), respectively, for a range of turbine inlet temperatures TIT (the highest TIT values exceed conventional practice but are included to examine the potential that would result from further improvements in turbine technology). On these graphs, the solid markers represent the Brayton cycle with regeneration, and the hollow markers show the results at which the specific pressure ratios do not allow regeneration. With regeneration, the cycle yields energy and exergy efficiencies of over 65% in the lower pressure ratio range; without regeneration they still reach over 55%. The observed behavior, including the existence of a value of π giving a maximal energy efficiency for a given TIT, is well known for Brayton cycles.

The same cycle parameters are used in the Ericsson and Brayton cycles for easy comparison. The number of Ericsson cycle expansion and compression stages in turbines and compressors, respectively, was chosen by gradually increasing them and examining the effect on the energy efficiency. As shown in Fig. 7, the energy efficiency increase tapers off as the number of stages increases; after the sixth stage, it only increases approximately 0.1% per stage added. All Ericsson cycles in this analysis were thus chosen to have six interstages in both the compressor and turbine.

Sample results are shown in Fig. 8 for a nitrogen Rankine cycle defined in Table 2. The thermal efficiency of

Table 3
The state properties of the computed Brayton cycle for the different working fluids

State	p	Ar			Ar–Xe			N_2			He			He–Xe			H_2		
		T	h	s	T	h	s	T	h	s	T	h	s	T	h	s	T	h	s
1	1	200	−52	−0.21	200	−34	−0.06	200	−103	−0.41	200	−510	−2.05	200	−263	−0.91	200	−1384	−5.57
2	8	505	107	−0.16	505	69	−0.03	391	96	−0.33	505	1076	−1.55	505	554	−0.66	395	1399	−4.47
3	8	714	216	0.02	714	141	0.09	902	653	0.57	714	2162	0.25	714	1114	0.27	870	8330	7.03
4	8	1500	626	0.41	1500	408	0.34	1500	1372	1.18	1500	6242	4.10	1500	3216	2.25	1500	18008	15.37
5	1	738	229	0.47	738	149	0.38	958	718	1.26	738	2282	4.73	738	1176	2.58	923	9107	16.48
6	1	528	119	0.30	527	78	0.27	452	161	0.44	529	1196	3.00	528	616	1.69	449	2176	5.96

Units: p [bar], T [K], h [kJ/kg], s [kJ/kg K].

Table 4
The state properties of the computed Ericsson cycle for the different working fluids

State	p	Ar			Ar–Xe			N_2			He			He–Xe			H_2		
		T	h	s	T	h	s	T	h	s	T	h	s	T	h	s	T	h	s
1	1	200	−52	−0.21	200	−34	−0.06	200	−103	−0.41	200	−509	−1.68	200	−263	−0.73	200	−1384	−5.57
2	8	233	−37	−0.57	233	−25	−0.3	223	−81.5	−0.93	246	−269	−5.2	245	−140	−2.55	224	−1049	−12.6
3	8	1216	478	0.30	1216	312	0.27	1275	1095	0.98	1217	4776	3.01	1217	2461	1.7	1268	14347	12.7
4	8	1500	626	0.41	1500	408	0.34	1500	1372	1.18	1500	6244	4.1	1500	3217	2.25	1500	18008	15.4
5	1	1325	535	0.78	1325	349	0.58	1392	1238	1.71	1325	5334	7.77	1325	2748	4.15	1384	16157	22.7
6	1	337	20	0.07	334	12.1	0.11	357	60.9	0.19	354	289	0.92	353	147	0.61	351	761	2.4

Units: p [bar], T [K], h [kJ/kg], s [kJ/kg K].

Table 5
The state properties of the computed Rankine cycle for the different working fluids

State	Ar				N_2			
	p	*T*	*h*	*s*	*p*	*T*	*h*	*s*
1	0.75	84	−275	−2.53	0.15	64	−457	−4.36
2	150	90	−263	−2.49	150	69	−436	−4.28
3	150	178	−154	−1.67	150	222	−136	−1.99
4	150	1500	632	−0.20	150	1500	1385	0.31
5	0.75	313	8	0.09	0.15	373	78	0.80
6	0.75	105	−101	−0.48	0.15	84	−223	−0.75

Units: *p* [bar], *T* [K], *h* [kJ/kg], *s* [kJ/kg K].

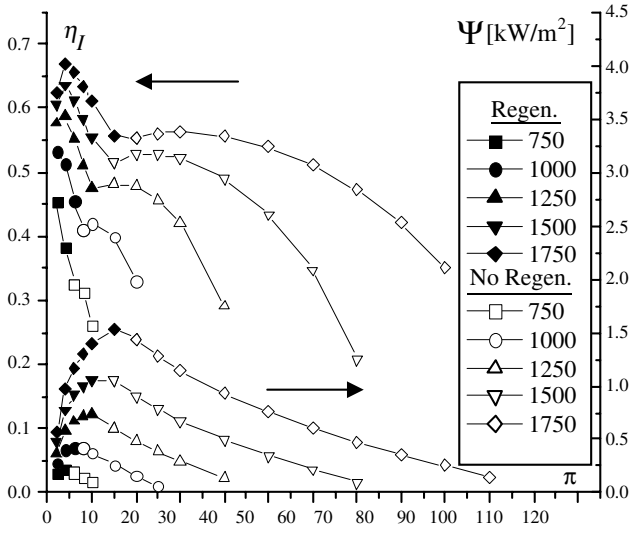

Fig. 5. Effect of pressure ratio on thermal efficiency and Ψ, argon Brayton cycle for cycles with regenerator (Regen.) and without (No Regen.), $p_L = 1$ bar.

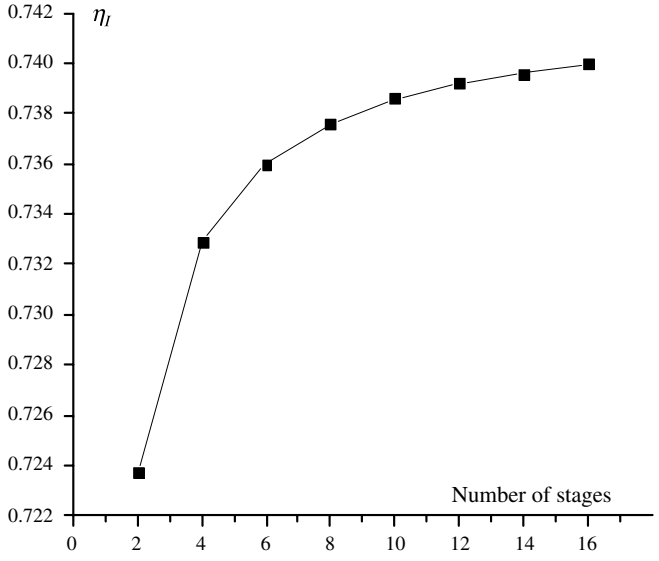

Fig. 7. Effect of the number of stages in turbine and compressor on η_I, argon Ericsson cycle, $p_L = 1$ bar, $\pi = 8$, TIT = 1500 K.

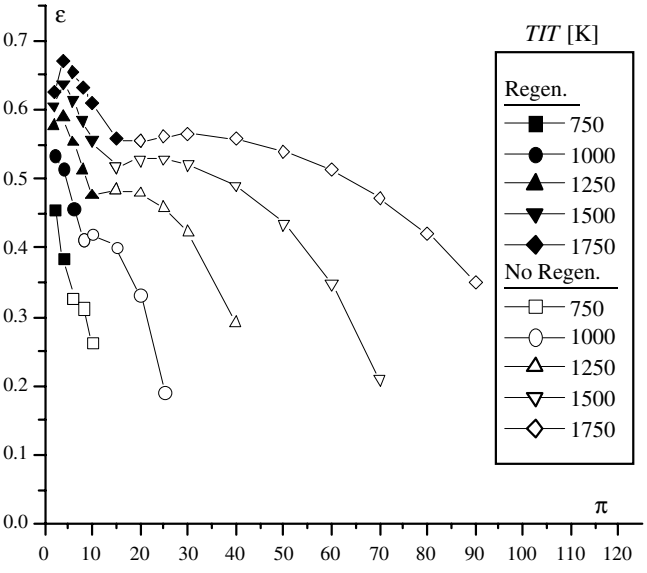

Fig. 6. Effect of pressure ratio on the exergy efficiency ε, argon Brayton cycle for cycles with regenerator (Regen.) and without (No Regen.), $p_L = 1$ bar.

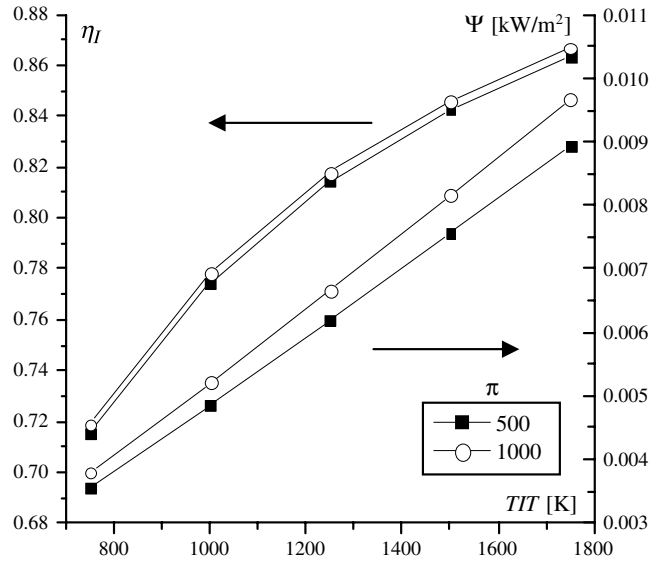

Fig. 8. Effect of TIT on thermal efficiency, nitrogen Rankine cycle, $p_L = 0.15$ bar.

Table 6
Back-work ratio, all cycles and working fluids [%]

Cycle	Ar	Ar–Xe	N_2	He	He–Xe	H_2
Brayton	39.94%	39.86%	30.31%	40.05%	40.05%	31.27%
Ericsson	17.12%	16.99%	17.17%	17.34%	17.33%	17.37%
Rankine	2.00%	N/A	1.57%	N/A	N/A	N/A

the Rankine cycle increases, as expected, with increasing TIT, and insignificantly with increasing π. The Rankine cycle has much higher energy and exergy efficiencies than the Brayton and Ericsson ones, reaching over 85% at the highest π, because of the much lower back-work ratio (see Table 6).

6.3. Radiator requirements

The analysis is conducted using Eqs. (3)–(8). It is assumed that $\epsilon = 1$, which can be approximately attained by proper exterior surface treatment. The heat transfer resistances, found in the denominator of Eq. (5), are shown in Table 7 for each working fluid. The gas to solid convective heat transfer coefficients h_c for the different working fluids of the Brayton and Ericsson cycles are found by using the Dittus-Boelter equation

$$h_c = \frac{0.023k}{\delta} Re^{0.8} Pr^{0.4} \tag{17}$$

where δ is the flow gap within the radiator. The Reynolds number (Re) was calculated assuming a fluid velocity of 1/3 the speed of sound, calculated based on fluid properties, to maximize h_c. The Brayton and Ericsson cycle heat transfer coefficients, and all parameters contributing to this calculation, are given in Table 8. When condensation takes place (Rankine cycle), it is known that the convective condensation heat transfer coefficient h_c is 10–100 times greater. It is noteworthy that the radiative heat transfer resistance is larger than the others by at least an order of magnitude, and thus better accuracy in determining the internal heat transfer coefficients, or attempts to increase them, will remain practically useless until ways to reduce the radiative resistance are developed. Since the radiative resistance depends primarily on the radiator temperature, the much higher resistances in the Rankine cycle reflect the lower radiator temperature in that cycle.

Table 8
Properties used in development of h_c for the Brayton and Ericsson cycles, at the average temperature

Property	Ar	Ar–Xe	N_2	He	He–Xe	H_2
c [m/s]	351	283	351	1106	794	1315
$c/3$ [m/s]	117	94	117	369	265	438
$Re \times 10^{-4}$	4.11	4.94	3.69	1.48	1.85	1.98
Pr	0.66	0.57	0.71	0.69	0.42	0.71
Nu	95.7	104.7	90.5	43.1	42.4	54.9
h_c [W/m^2 K]	344	293	471	1292	1188	1976

7. Comparison of working fluid effects on system performance

Since a sensitivity analysis of the Brayton cycle showed that the highest energy efficiencies and Ψ are obtained at about TIT = 1500 K (the highest assumed in this study for all working fluids) and $\pi = 8$, the comparison between the Brayton and Ericsson cycles is conducted up to these temperature and pressures. Sample T–s diagrams for the different working fluids of the Brayton cycle are shown in Figs. 9 and 10. Ericsson cycle T–s diagrams are shown in Figs. 11 and 12, and it is important to note that this cycle configuration is specific to this analysis and that Ericsson configurations can vary based on number of interstages in the turbine and compressor. The Rankine cycle has the

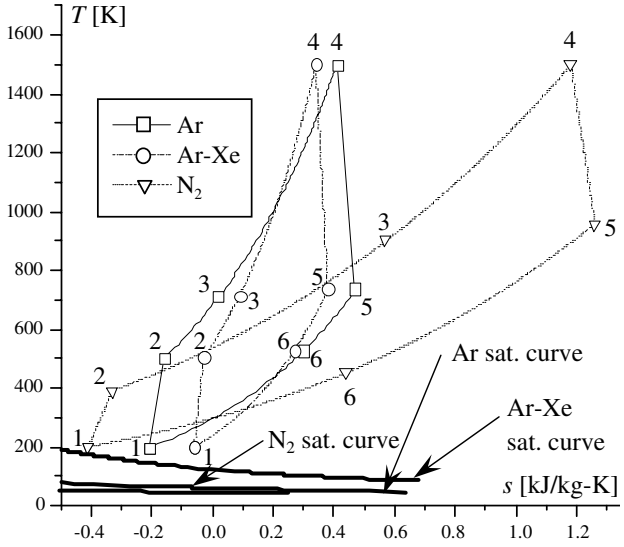

Fig. 9. Brayton cycle T–s diagrams (Ar, Ar–Xe, and N_2), $p_L = 1$ bar, $\pi = 8$.

Table 7
Radiator heat transfer resistances [m^{2}K/W] ($R_{t,\text{radiative}}$ in the Ericsson cycle varies among the compression interstage heat exchangers)

Cycle	Resistance	Ar	Ar–Xe	N_2	He	He–Xe	H_2
Brayton, Ericsson	$R_{t,\text{internal}}$	$2.9(10^{-3})$	$3.4(10^{-3})$	$2.1(10^{-3})$	$7.7(10^{-3})$	$8.4(10^{-4})$	$5.1(10^{-4})$
	$R_{t,\text{wall}}$	$1.3(10^{-4})$	$1.3(10^{-4})$	$1.3(10^{-4})$	$1.3(10^{-4})$	$1.3(10^{-4})$	$1.3(10^{-4})$
Brayton	$R_{t,\text{radiative}}$	0.47	0.47	0.61	0.46	0.46	0.62
Ericsson	$R_{t,\text{radiative}}$	1.00–1.79	1.01–1.79	0.91–1.92	0.92–1.65	0.92–1.65	0.93–1.91
Rankine	$R_{t,\text{radiative}}$	22.42	N/A	47.74	N/A	N/A	N/A

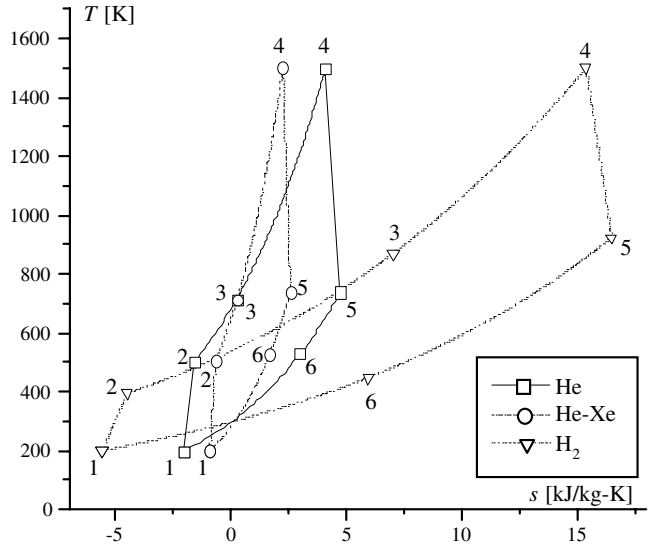

Fig. 10. Brayton cycle T–s diagrams (He, He–Xe, and H_2), $p_L = 1$ bar, $\pi = 8$.

highest η_I and Ψ at TIT = 1500 K and $p_H = 150$ bar which are the base parameters for comparisons (note: this implies $\pi = 200$ for Ar and $\pi = 1000$ for N_2). Further increase in π does not significantly increase η_I (see Fig. 8): doubling π increases η_I by only 0.3%. η_I, ε, and Ψ all increase with increasing TIT and π for both working fluids used in the Rankine cycle. Sample T–s diagrams for the Rankine cycle are shown in Fig. 13. Fig. 14 shows the summary of the performance analysis results.

Compared with computed cycles operating under terrestrial conditions, the space cycles are more efficient, as expected due to the lower temperature heat sink. In addition, the Brayton cycle using Ar, Ar–Xe, He, and He–Xe, operating at the lower temperature of space, allows regeneration otherwise impossible at terrestrial conditions due to temperature constraints. As a result, efficiencies increase by 45%. Likewise, using N_2 and H_2, using regeneration both in space and on earth, have efficiency increases of over 28%. Similarly, Ericsson cycles gain an efficiency increase of over 14% for all working fluids considered when operating in space. Although yielding higher efficiencies both in space and on Earth, space Ericsson cycles have a slightly lower increase in efficiency over terrestrial ones because they are already highly efficient in being close to the ideal Carnot cycle by design (52–56% thermal efficiency at terrestrial conditions). Currently, state of the art operating terrestrial power plants have thermal efficiencies of 40% for gas turbine power (100 MW) amazingly close to those predicted in our simplified analysis (Table 2), nearly 50% for conventional steam power plant (1000 MW), and 60% for a combined cycle (1000 MW) [28,29], all lower than the predicted space power cycles. It is noteworthy that a space Rankine cycle is predicted to attain efficiency in the range of 80% just by itself, not in a combined configuration. A combined configuration is unnecessary anyway because the heat rejection is at the lowest possible temperatures.

Aside from the Brayton terrestrial cycles with compressor exit temperatures that are too high to use regeneration (monatomic gases), all terrestrial cycles have higher exergy efficiencies compared to their respective space cycle (Table 2). Comparison of the exergy efficiency of terrestrial and space cycles is not straightforward, because of the different dead states used for them: $T_0 = 288.2$ K for terrestrial cycles, and $T_0 = 2.7$ K for space. Some interesting conclusions can be drawn though: examination of the exergy efficiency definition, Eq. (2), leads upon expansion to

$$\varepsilon = \frac{w_{net}}{(a_{out} - a_{in})_{heat\text{-}addition}} = \frac{w_{net}}{q_{in} - T_0(s_{out} - s_{in})_{heat\text{-}addition}} \tag{18}$$

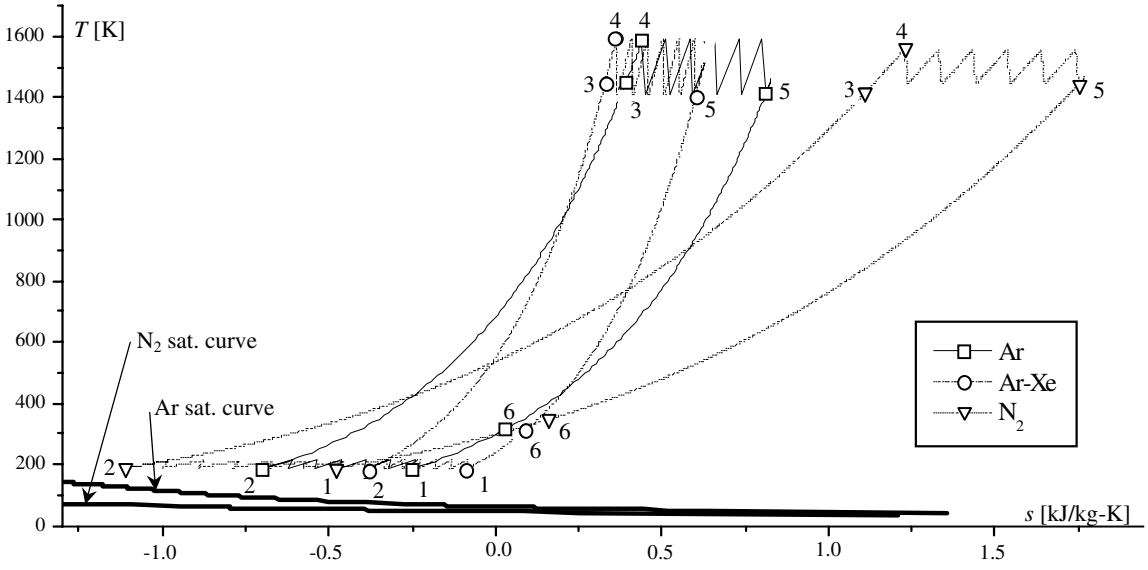

Fig. 11. Ericsson cycle T–s diagrams (Ar, Ar–Xe, and N_2), $p_L = 1$ bar, $\pi = 8$.

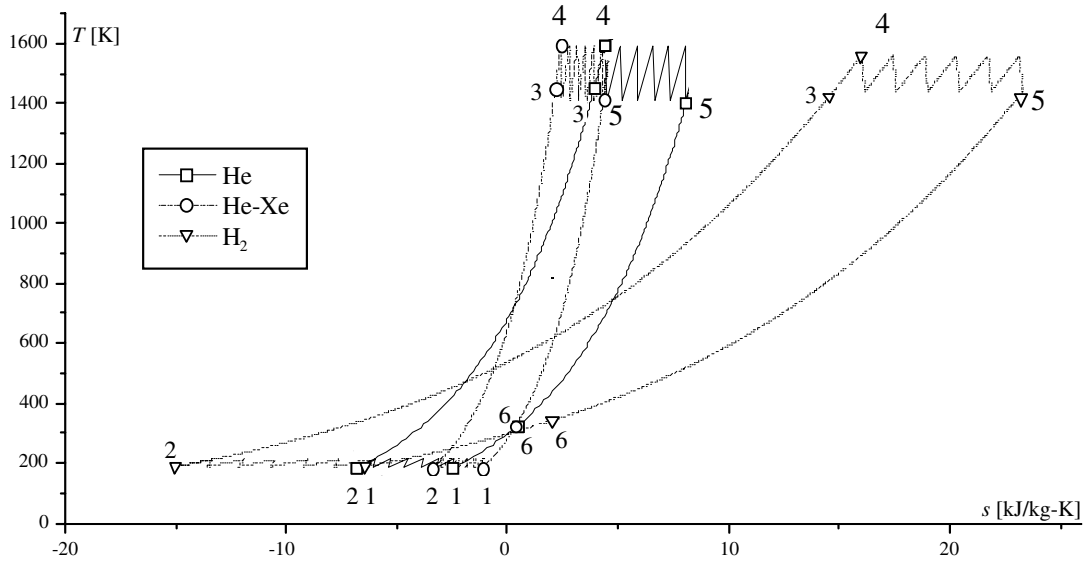

Fig. 12. Ericsson cycle T–s diagrams (He, He–Xe, and H_2), $p_L = 1$ bar, $\pi = 8$.

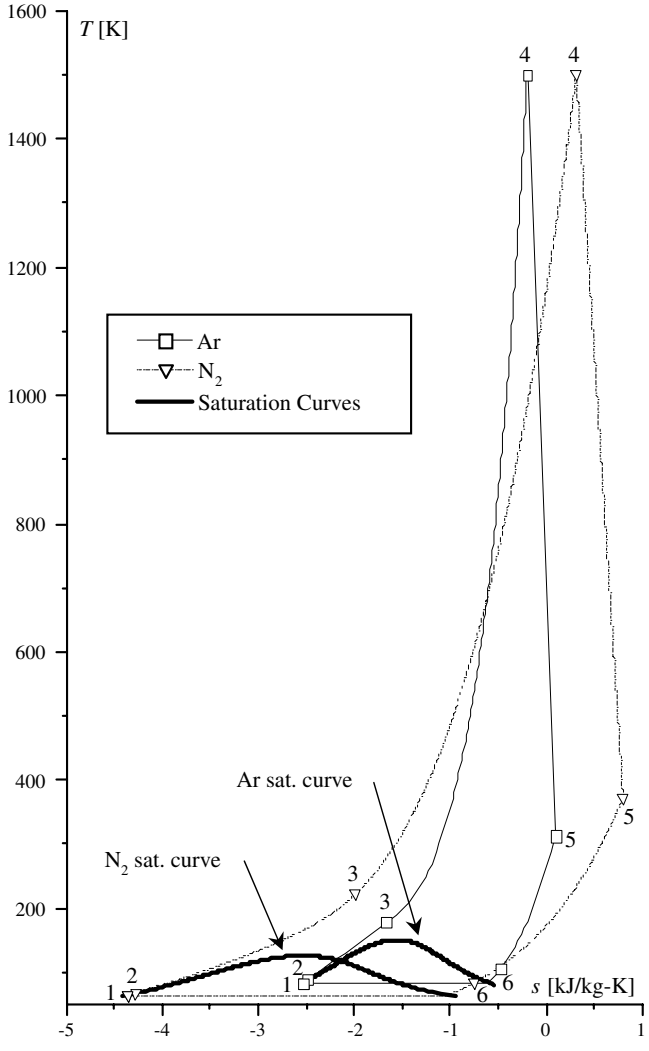

Fig. 13. Rankine cycle T–s diagrams, Ar: $p_L = 0.75$ bar, $\pi = 200$, N_2: $p_L = 0.15$ bar, $\pi = 1000$.

indicating that for the same heat input and work output, ε would be higher for the terrestrial cycle than the space one because of the much higher assumed T_0, and thus the much lower exergy of the heat input. Looking at it in another way, choice of the very low T_0 as it is in space brings the exergy efficiency very close to the energy efficiency. Because the dead state of terrestrial cycles is at $T_0 = 288.2$ K, the cycle has utilized all of the heat available relative to its surroundings. In space, the heat sink is much lower, reducing the exergy efficiency to approximately the value of the energy efficiency. This shows that it is possible to decrease the low temperature of the space cycle, which will lead to improvements in the efficiency.

The effect of the working fluid when used in Brayton cycles is as expected, where with N_2 and H_2 they have about 9% higher efficiencies than with other fluids because of their lower values of $(1 - c_v/c_p)$ as shown by Eq. (10). The Ericsson cycle energy and exergy efficiencies are more complex to explain as indicated by Eq. (11). The value of $(c_{p,L}\Delta T_L/c_{p,H}\Delta T_H)$ is about 0.18 for Ar, N_2 and H_2, but it reaches 0.26 for He, results to lower efficiency for the cycle with He as the working fluids. The remaining significant term is the first term in the denominator ($\Delta T_{HS}/\Delta T_H$), since n is constant. For diatomic gases H_2 and N_2, ΔT_H and ΔT_L are smaller. Smaller ΔT_H and ΔT_L produce a larger temperature range for regeneration. For fixed regenerator effectiveness (0.9), more heat is recovered in the regenerator and raises the regenerator outlet temperature T_3 to a higher level. The heat demand in HS is thus reduced with smaller ΔT_{HS}.

For the Brayton cycle, Ψ for N_2 and H_2 is about 14% lower than that of the other working fluids. It can be explained by using Eq. (8): the cycle bottom temperatures using N_2 and H_2 are lower, thus leading to a (a) 9% higher η_I, which tends to raise Ψ but also (b) 32% higher thermal

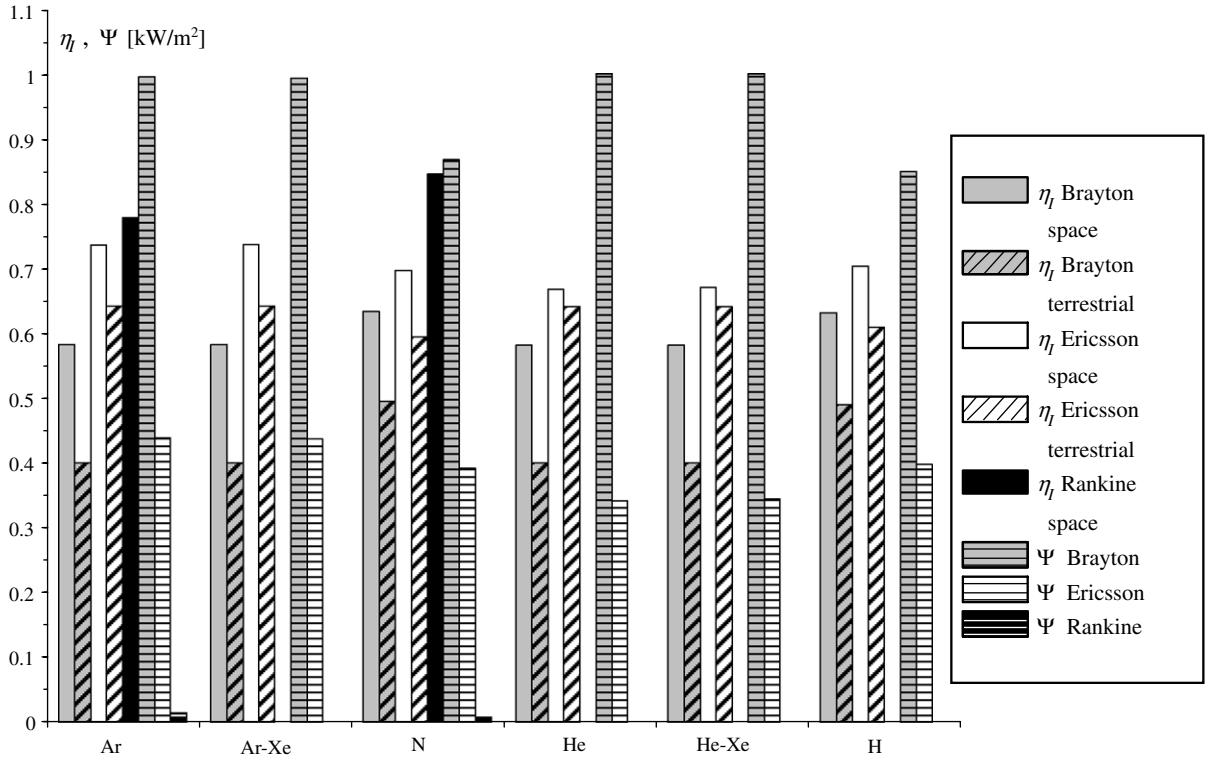

Fig. 14. Computed η_I and Ψ of the space and terrestrial cycles for the different working fluids. Note: Ψ for the Rankine cycle was computed only for Ar and N_2 and is imperceptibly small here, the values are in Table 2.

resistance of the radiator by about 32% (Table 7) and hence 32% lower value of U, as well as a lower value of ΔT_{lm}, both of which reduce Ψ more. Similarly in the Rankine cycle, in which the bottom temperatures are even lower, these decreases in U and ΔT_{lm} for the cycle using N_2 are stronger than the effect of increased efficiency, causing it have a lower Ψ than the cycle using Ar. Summarizing, in the Brayton and Rankine cycles the working fluids that exhibit highest η_I (the diatomic ones) have the lowest values of Ψ.

In contrast, for Ericsson cycles, the working fluids the relationship between η_I and Ψ is directly proportional, where cycles using fluids that have a higher η_I also have a higher value of Ψ.

While the Rankine cycle efficiency is the highest, its bottom temperature is lowest, here resulting in a Ψ that is over 100 times smaller than that for the Brayton and Ericsson cycles. Using Ar gives a Ψ that is about 76% greater than that when using N_2 in the Rankine cycle. This occurs because Ar has a greater values of U and ΔT_{lm} (affecting Eq. (8)), a direct result of less heat recuperated in the regenerator since $(1 - c_v/c_p)$ is greater than that of diatomic gases, lowering turbine exit temperature and thus the amount of heat available for regeneration. These increases in U and ΔT_{lm} are stronger than the effect of the efficiency in Eq. (8), which causes Ar to have higher Ψ than N_2 in the Rankine cycle.

The Rankine cycle has the highest exergy efficiencies because its T_L is closest to the dead state (Table 2), and Brayton cycles have the lowest because they operate furthest from the dead state. Brayton cycle efficiencies can be improved by lowering the T_L of the cycles. Ericsson cycles have higher ε than Brayton due to higher η_I, but lowering the cycle T_L is difficult because it approaches saturation temperature for Ar, Ar–Xe, and N_2 due to the temperature difference between interstages in the compressor during intercooling stages (Fig. 11).

8. Conclusions

Thermal power cycles, developed with space-based application in mind, were modeled and optimized for various working fluids. The analysis shows that:

1. Under the examined conditions, the thermal efficiency of Brayton cycles reaches 58–63%, Ericsson 69–74%, and Rankine 78–85% (see Fig 14).
2. These efficiencies are significantly higher than those for the computed or real terrestrial cycles: by up to 45% for the Brayton, 17% for the Ericsson, and remarkably 44% for the Rankine cycle even when compared with the best terrestrial combined cycles.
3. From the considered working fluids, the diatomic gases (N_2 and H_2) produce somewhat better efficiencies than the monatomic ones in the Brayton and Rankine cycles.
4. Although Rankine cycles have higher thermal and exergy efficiencies, they require much larger radiator areas because they also reject heat at much lower temperatures

and their radiators thus have much lower radiative heat transfer coefficients and operate with much smaller temperature differences. As a result, the Rankine cycles on average have lower Ψ, approximately 4% of that obtained for Ericsson cycles, and only 1% of that for Brayton cycles.

References

[1] Glaser PE, Davidson FP, Csigi KI. Solar power satellites – the emerging energy option. New York: Ellis Horwood; 1994.

[2] Mankins JC. Space solar power: a major new energy option? J Aerospace Engng 2001;14(2):38–45.

[3] Mankins JC. Space solar power option. Aerospace Am 1997;35(5):30.

[4] Lior N. Power from space. Energy Convers Manage 2001;42(15–17): 1769–805.

[5] Hoffert MI, Caldeira K, Nozette S. Evolutionary paths to orbital power & light. In: 50th Int astronautical cong, 1999.

[6] Strickland JK. Advantages of solar power satellites for base load electrical supply compared to ground solar power. Solar Energy 1996;56(1):23–40.

[7] Canough G. Space solar power vs terrestrial solar power. Space Energy Transport 1997;2(2):127–55.

[8] Hoffert MI, Potter SD. Beam it down. Technolo Rev 1997;100(7):30.

[9] Nansen RH. Wireless power transmission: the key to solar power satellites. IEEE AES Syst Mag 1996;11(1):33–9.

[10] Leonard RS. The lack of high quality energy results in significant environmental degradation. Solar Energy 1996;56(1):62–7.

[11] Nagatomo M. An approach to develop space solar power as a new energy system for developing countries. Solar Energy 1996;56(1): 111–8.

[12] Glaser PE. Guest editorial: solar energy for planet Earth. Solar Energy 1996;56(1):1–2.

[13] Weingartner S, Blumenberg J. Solar power satellite – life-cycle energy recovery considerations. Acta Astronaut 1995;35(9-11):591–9.

[14] Harper WB, Boyle B, Kudija CT. Solar dynamic CBC power for space station Freedom, ASME paper 90-GT-78, NY,1990.

[15] Wu Yu-Ting, Ren Jian-Xun, Guo Zeng-Yuan, Liang Xin-Gang. Optimal analysis of a space solar dynamic power system. Solar Energy 2003;74(3):205–15.

[16] Assis AKT, Neves MCD. History of 2.7 K Temperature prior to Penzias and Wilson. APEIRON. 3, 2. p. 79–84.

[17] NASA Goddard Space Flight Center. http://library.gsfc.nasa.gov/GSFCHome.htm.

[18] Nichols LD. Comparison of Brayton and Rankine cycle magneto-gasdynamic space-power generation systems. NASA TN D-5085, NASA, Washington, DC, March 1969.

[19] Thomas S. Effects of the earth orbit environment on thin-wall bubbles. J Spacecraft Rockets 1990;27(4):438–45.

[20] NASA National Space Science Data Center. See also http://nssdc.gsfc.nasa.gov/.

[21] Shaltens RK, Boyle RV. Initial results from the solar dynamic (SD) ground test demonstration (GTD) project at NASA Lewis. In: Proc. 30th IECEC ASME, Orlando, 1995.

[22] Shepard NF et al. 20-kWe space reactor power system using Brayton cycle conversion. Proc. 11th Symp. on Space Nuclear Power and Propulsion, Albuquerque, NM, USA,1994.

[23] Agazzani A, Massardo A. Advanced solar dynamic space power systems, Part I: Efficiency and surface optimization. ASME J Solar Energy Engng 1995;117(4):265–74.

[24] Agazzani A, Massardo A. Advanced solar dynamic space power systems, Part II: Detailed design and specific parameters optimization. ASME J Solar Energy Engng 1995;117(4):274–81.

[25] Hanlon C. Feasibility of demonstration solar dynamics on space station. In: Proc. 29th IECEC Part 2, 1994.

[26] Shaltens RK, Mason LS. Early results from solar dynamic space power system testing. J Propulsion Power 1996;12(5):852–8.

[27] Aspen Plus®, Aspen Technology, Inc., version 12.1, http://www.aspentech.com/.

[28] Rukes B, Taud R. Status and perspectives of fossil power generation. Energy 2004;29(12–15):1853–74.

[29] Valenti M. Reaching for 60 percent. Mech Eng 2002;124(4):35–9.